Heliyon 9 (2023) e20976

Contents lists available at ScienceDirect

Heliyon

journal homepage: www.cell.com/heliyon

Montmorillonite modified Ni/Mg/Al ternary layered double hydroxide nanoflowers with enhanced adsorption features

Tayyaba Waheed [a], Pu Min [a,*], Salah ud Din [b], Pervaiz Ahmad [c], Mayeen Uddin Khandaker [d,e], Sirajul Haq [b], K.S. Al-Mugren [f], Fazal Ur Rehman [b], Bilal Akram [g], Sehrish Nazir [b]

[a] *State Key Laboratory of Chemical Resource Engineering, Beijing Engineering Center for Hierarchical Catalysts, Beijing University of Chemical Technology, No. 15 Beisanhuan East Road, Chaoyang District, Beijing, 100029, China*
[b] *Department of Chemistry, University of Azad Jammu and Kashmir, Muzffarabad, 13100, Pakistan*
[c] *Department of Physics, University of Azad Jammu and Kashmir, 13100, Muzaffarabad, Pakistan*
[d] *Centre for Applied Physics and Radiation Technologies, School of Engineering and Technology, Sunway University, 47500, Bandar Sunway, Selangor, Malaysia*
[e] *Department of General Education Development, Faculty of Science and Information Technology, Daffodil International University, D.I.U. Rd., Dhaka, 1341, Bangladesh*
[f] *Physics department, Science College, Princess Nourah bint AbdulRahman University, Riyadh, 11144, Saudi Arabia*
[g] *Department of Chemistry, Women University of Azad Jammu and Kashmir, Pakistan*

ARTICLE INFO

Keywords:
Layered double hydroxide
Methyl orange
Congo red
Adsorption

ABSTRACT

A hydrothermal technique was employed to synthesize Ni/Mg/Al ternary L.D.H.s modified with montmorillonite (NMA-MMT-LDHs). Many characterization methods, including X-ray diffraction (XRD), scanning electron microscopy (S.E.M.), Fourier transform infrared (FTIR), and Brunauer, Emmett, and Teller (B.E.T.), were used to assess the physiochemical properties of the produced analytes. Congo red and methylene blue were utilized as model dyes to treat textile waste with the synthesized analytes. The batch adsorption model was utilized to conduct the adsorption experiments under varying contact time, adsorbent dosage, and solution pH conditions. A pseudo-second-order kinetics and the Langmuir adsorption model control the adsorption process. The maximum monolayer adsorption capacities of C.R. and M.B. were determined to be 344 and 200 mg/g, respectively. As the quantity of dosage increased from the 0.01–0.04 g, the percent removal efficiency (%) increased from 75 to 87 % for S2-LDH, 84–88 % for S2-MMT, 86–93 % for S3-MMT, and 95–97% for S4-MMT for C.R. dye and 82–85 % for S2-LDH, 83–89 % for S2-MMT, 83–91 % for S3-MMT, and 84–92 % for S4-MMT for M.B. dye. The removal percentage of C.R. dye for adsorbents S2-LDH, S2-MMT, S3-MMT, and S4-MMT were 75 %, 84 %, 86 %, and 95 %, respectively and 82 %, 83 %, 83 %, and 85 %, respectively for the M.B. dye removal. The presence of MMT significantly increases the affinity of Ni/Mg/Al-LDHs (NMA-LDHs), and the designed production technique can be used to produce a variety of compositionally distinct adsorbent materials.

* Corresponding author.
E-mail addresses: 2018420013@mail.buct.edu.cn (T. Waheed), pumin@mail.buct.edu.cn (P. Min), salah.mahsud@ajku.edu.pk (S. Din), pervaiz.ahmad@ajku.edu.pk (P. Ahmad), mayeenk@sunway.edu.my (M.U. Khandaker), siraj.ulhaq@ajku.edu.pk (S. Haq), ksalmogren@pnu.edu.sa (K.S. Al-Mugren), fazal.rehman@ajku.edu.pk (F.U. Rehman), bai-l16@tsinghua.org.cn (B. Akram), sehrishnazir870@gmail.com (S. Nazir).

https://doi.org/10.1016/j.heliyon.2023.e20976
Received 7 June 2023; Received in revised form 6 October 2023; Accepted 12 October 2023
Available online 14 October 2023
2405-8440/© 2023 The Authors. Published by Elsevier Ltd. This is an open access article under the CC BY-NC-ND license (http://creativecommons.org/licenses/by-nc-nd/4.0/).

1. Introduction

Clean water has become a precious and locally rare resource due to rapid development. Water is being polluted through human activities that may cause various waterborne diseases. The majority of waste material is coloured, notably dyes [1]. The textile, leather, paint, tanneries, paper, and plastic industries all rely heavily on synthetic dyes, which are produced more than 7×10^5 tonnes annually [2]. Methylene blue (M.B.) is a textile dye that is commonly used to color paper, silk, wool, cotton and other textiles. Beyond its use in medicine, M.B. in water poses several threats to human health [3,4]. M.B. dye contamination in water bodies has increased over the past few decades, which is a severe issue, due to widespread application of M.B. dye in the textile sector and the uncontrolled release of wastewater [5]. Consuming water polluted with M.B. dye is unhealthy for people and weakens their immune systems, causing symptoms including vertigo and delusions in the brain [6]. Like these dyes, Congo-red dye (C.R.) is mainly used to dye industrial products [7]. The extensive usage of azo dyes results in significant wastewater production that contains azo dye contaminants. Because C.R. (diazo dye) contains an aromatic amine, it is known to be carcinogenic, and due to their aromatic compositions, azo dyes are resistant to natural degradation. Dye pollution affects wildlife and plants negatively and persists in the environment for a long time [8].

Many studies have looked into eliminating dyes from wastewater utilizing various processes, including photochemical degradation, microbial degradation, chemical oxidation, reverse osmosis, flotation process, and adsorption. Adsorption is one of these ways that is most efficient for eliminating dyes [9]. It is the most cost-effective method because many adsorbents are available, it is easy to design, highly efficient, and can deal with dyes in concentrated form [10]. The suitable adsorbent must be chosen to achieve the best adsorption performance. C.N.T.s, red mud, chitosan, fly ash, rice husk, peat, ferrite nanoparticles, and maize stalk have all been investigated for the removal of colorful dyes from wastewater. Developing new, cost-effective, and efficient adsorbent materials is still demanding [11]. Layered double hydroxide (L.D.H), also known as anionic clays or hydrotalcite-like compounds, has drawn considerable interest due to its potential applications in various industries, like water treatment [12]. The structure of these solids is derived from the structure of brucite, where trivalent cations largely replace divalent ones. $[M^{2+}_{(1-x)}\, M^{3+}_{x}\, (OH)_2]^{x+}\, (A^{n-})_{(x/n)} \times mH_2O$ is the general formula for L.D.H.s, where M^{2+} is a divalent cation, M^{3+} is a trivalent cation, A is an interlayer anion, and x is a ratio of divalent to trivalent cations with values ranging from 0.2 to 0.33. The $M(OH)_6$ octahedra that shared their edges formed layers that resembled brucite. It's worth noting that a partial and isostructural M^{2+} to M^{3+} replacement would result in positive charges across these layers, which would be balanced by a negatively charged interlayer space made up of anions and water molecules [13]. L.D.H.s have several distinguishing characteristics that allow them to be used as adsorbents, notably interlayer anion exchange capacity, a large surface area, and positively charged surfaces [14]. However, the adsorptive efficiency of L.D.H. can be increased further through structural and compositional modifications. Montmorillonite (MMT) is a clay mineral in which one Al^{3+} octahedral sheet is linked to two Si^{4+} tetrahedral sheets. Many inorganic cations can simply incorporated into MMT layers and remove the negative species. According to several research, MMT is a promising solution for the removal of cationic dyes. As a result, we may conclude that an adsorbent consisting of L.D.H. with MMT can remove anionic as well as cationic dyes from wastewater [15]. Tarmizi et al. published a report on the fabrication and analysis of a montmorillonite-mixed metal oxide composite and its anionic and cationic dye removal adsorption capacities [16]. Al Nasrawi et al. discovered that a CuMgAl-LDH/MMT nanocomposite improved Cd^{2+} removal [17]. Al Nasrawi and coworkers explored the adsorptive behavior of a CuMgAl-LDH/MMT nanocomposite to remove Zn(II) ion from an aqeous solution [18].

Herein, we demonstrate the synthesis of ternary NMA-LDH modified by MMT utilizing the simple hydrothermal method. To the best of our knowledge, research on the synthesis of NMA-MMT-LDHs, as well as their cationic and anionic adsorption capabilities is currently not well investigated. The as-synthesized NMA-MMT-LDHs were studied using XRD, FT-IR, S.E.M., and B.E.T., and it was subsequently used as an adsorbent to trap model textile waste. In a batch experiment, variables such as effect of initial pH, contact time and initial concentration of dyes on adsorption performance were examined.

2. Experimental work

2.1. Materials and reagents

Nickel nitrate $Ni(NO_3)_2.6H_2O$ (98.5 % pure), magnesium nitrate $Mg(NO_3)_2.6H_2O$ (99.9% pure), aluminum nitrate $Al(NO_3)_3.9H_2O$ (98.5 % pure), Urea [C.O. $(NH_2)_2$] (93 % pure), sodium hydroxide (NaOH) (97.0 % pure), C.R. and M.B. were obtained from Xilong Science Co., Ltd. Na-MMT obtained from Zhejiang Sanding Technology Co., Ltd. The chemicals utilized in experiments were all of analytical quality and didn't need to be further purified. In every step of the experiment, deionized water was used. In the current investigation, C.R. and M.B. were used as adsorbates.

2.2. Synthesis of L.D.H. And MMT-LDHs

Synthesis of NMA-LDH adsorbent was carried out by dissolving 0.01 M of $Al(NO_3)_3.9H_2O$, 0.01 M of $Mg(NO_3)_2.6H_2O$ and 0.01 M of $Ni(NO_3)_2.6H_2O$ in 30 mL of deionized water. Urea (0.04 M) was used as a co-precipitating agent. Light green precipitates appeared after a hydrothermal reaction at 120 °C for 24 h. Then, the solution was filtered, washed, and dried. The chemical ratio of metals $(Ni^{+2} + Mg^{+2})/Al^{3+}$ were taken as 2. Similarly, NMA-LDHs with different metallic ratios 3 and 4 were also synthesized by the same method and labeled as S2-LDH, S3-LDH, and S4-LDH.

The NMA-MMT-LDHs were synthesized in a single step using a hydrothermal technique. In particular, 1g of Na-MMT was dispersed

in a 100 mL beaker with 30 mL of deionized water. After 10 min of stirring. $Mg(NO_3)_2.6H_2O$, $Al(NO_3)_3.9H_2O$, $Ni(NO_3)_2.6H_2O$, and urea were added, and the mixture was stirred for a further 10 min. The resulting slurry was placed in a Teflon autoclave that was kept at 120 °C for 24 h. The resulting precipitates formed were vacuum filtered and dried overnight at 60 °C. The following is a hypothetical reaction mechanism (Eq. (1) - Eq. (4)) [19]:

$$CO(NH_2)_2 + 3H_2O \rightarrow 2OH^- + 2NH_4^+ + CO2 \tag{1}$$

$$CO_2 + 2H_2O \rightarrow CO_3^{2-} + 2H+ \tag{2}$$

$$Mg^{2+} + Al^{3+} + Ni^{2+} + OH^- + CO_3^{2-} \rightarrow NiMgAl - CO_3^{2-} - LDH \tag{3}$$

$$NiMgAl - CO_3^{2-} - LDH + MMT \rightarrow NiMgAl - MMT - LDH \tag{4}$$

Urea can break down into ammonia gas (NH^{4+}) and carbon dioxide (CO_2) in hydrothermal environment. Then, by adding water, it converted into CO_3^{2-} and O.H.$^{\cdot}$. Finally, NMA-LDHs were formed and then modified with MMT to form NMA-MMT-LDHs.

The synthesis of NMA-LDHs and fabrication process on the MMT is shown in Scheme 1. The total feeding ratios of $(Ni^{+2} + Mg^{+2})/Al^{3+}$ were 2, 3, and 4, respectively, and the samples were labeled as S2-MMT, S3-MMT, and S4-MMT, respectively.

2.3. Characterization of the products

The X-ray diffraction (XRD) pattern of the products was obtained on an X-Ray Diffractometer Shimadzu (XRD-6000) using a Cu Kα radiation source (λ = 1.5406 Å). A scanning electron microscope (S.E.M., Hitachi S-4800) was used to examin the sample morphologies and elemental mapping. Nitrogen adsorption/desorption was carried out at 77 K on the Micrometrics ASAP 2460 volumetric analyzer to determine specific surface area, porosity, and pore diameter. Fourier transform infrared spectroscopy (FT-IR Nicolet 8700) was used for the analysis of functional groups. The dyes concentrations (C.R. and M.B.) were determined by using UV–Vis spectrophotometer (Shimadzu UV-2501 PC).

2.4. Adsorption test

Adsorption tests were conducted to determine the effects of contact time, pH, and adsorbent dosage. These tests were conducted using 10 mg of each produced substance in 250 mL beakers with 100 mL of 25 mg/L C R. and M.B. solutions with pH values ranging from 2 to 10. By adding NaOH (0.1 M) or HNO_3 (0.1 M), the pH of the solution was brought to the proper values. After that, G.L.P. 21 pH meter was used to determine the pH. The suspension of samples was taken out at each interval of 5 min, and the final concentrations of C.R. and M.B. were calculated using a UV–visible spectrophotometer with maximum wavelengths of 497 nm and 664 nm, respectively. The dosage effect was studied by adjusting the dosage of each sample (10–40 mg) while mixing C.R. and M.B. solution (25 mg/L) in separate 250 mL beakers.

Eqs. (5) and (6) were used to calculate the percent removal (%) and the maximum amount adsorbed (mg/g):

$$\text{Removal } \% = \frac{(C_o - C_e)}{C_e} \times 100 \tag{5}$$

$$q_t = \frac{(C_0 - C_t)V}{m} \tag{6}$$

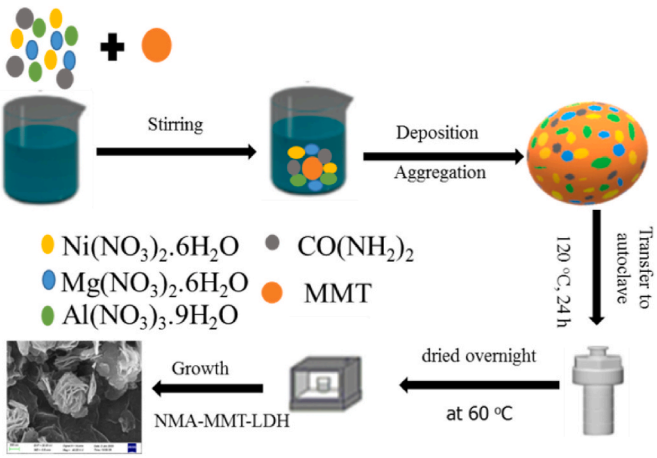

Scheme 1. Representation of NMA-LDH and NMA-MMT-LDH synthesis.

2.5. Kinetics studies

In order to conduct adsorption kinetic experiments for C.R. and M.B., 10 mg of samples were added to 250 mL beakers containing 100 mL of dyes at pH = 2 ± 0.2 for C.R. (25 mg/L) and pH = 9 ± 0.2 for M.B. At room temperature, the beaker was sealed and constantly stirred. A UV spectrophotometer (SHIMADZU UV-2501PC) was used to measure the concentrations of C.R. and M.B. dyes in the aqueous samples at their maximum absorption wavelengths of 497 nm and 664 nm, respectively. Using Eq. (7), the adsorbed amount (q_t) of both the dyes on the prepared samples was determined.

$$q_t = \frac{(C_o - C_t) \times V}{m} \tag{7}$$

where q_t (mg/g) represents the quantity of dye adsorbed at contact time t (min.), C_0 (mg/L) represents the initial dye concentration, C_t (mg/L) represents the concentration at contact time t, V (L) represents the volume of solution, and m (g) adsorbent's mass.

The mechanism of the controlled adsorption process was studied using pseudo-first-order and pseudo-second-order kinetic models [15,16]. The linear expressions for these kinetic models are given in Eqs. (8) and (9), respectively. Where k_1 (min^{-1}) represents the fictitious first-order constant and k_2 (g/mg min) represents the fictitious second-order kinetic rate constant, q_e (mg/g) denotes the amount adsorbed at quilibrium, and q_t (mg/L) is the amount adsorbed at time t.

$$\ln(q_e - q_t) = \ln q_e - k_1 t \tag{8}$$

$$\frac{t}{q_t} = \frac{1}{k_2 qe^2} + \frac{t}{q_e} \tag{9}$$

2.6. Adsorption isotherm

In order to ascertain the materials' maximal adsorption potential at different concentrations (5–25 mg/L), adsorption isotherm conduct tests were performed. 0.01 g of samples were mixed in 100 mL of C.R. and M.B. solutions (5–25 mg/L) for 80 min while being constantly stirred at 25 °C to calculate the rest of the concentration of C.R. and M.B. using a U.V. spectrophotometer. Eq. (7). was used to calculate removal capacity of the prepared samples for C.R. and M.B. dyes. Eqs. (10) and (11) were applied to fit both Langmuir and Freundlich isotherm models to the collected data.

$$\frac{C_e}{q_e} = \frac{C_e}{q_{\max}} + \frac{1}{q_{\max} K_L} \tag{10}$$

$$\ln q_e = \ln K_F + \frac{1}{n} \ln C_e \tag{11}$$

where C_e (mg/L) is the concentration at equilibrium, q_e (mg/g) shows the removal capacity at equilibrium, and q_{max} (mg/g) represents the potential maximum adsorption capacity. K_L is the Langmuir constant, K_F is the Freundlich constant, and 1/n is the heterogeneity factor [20]. From Eq. (12), it is possible to determine the Freundlich model's maximal removal capacity.

$$K_F = \frac{q_m}{C_o^{1/n}} \tag{12}$$

Eq. (13) was used to get the separation factor (R_L). R_L was employed to investigate the adsorption nature and shape of Langmuir isotherm;

$$R_L = \frac{1}{1 + K_L C_o} \tag{13}$$

2.7. Regeneration cycle

Adsorbents reusability is an essential aspect of their practical use. Adsorption-desorption treatment cycles were performed to assess the reusability of each sample. 1g of each sample was added to 50 mL of 25 mg/L of C.R. and M.B. solutions, which were shaken at 150 rpm. After C.R. and M.B. dyes adsorption, samples were collected and washed with 20 mL of 8 % HNO_3 to eliminate the remaining C.R. and M.B. dye. Before being utilized in the next adsorption cycle, the samples were repeatedly washed with distilled water to remove excess acid and then dried at 100 °C. The adsorption-desorption cycles were repeated by using the same adsorbents [21].

3. Results and discussion

3.1. X-ray diffraction

Fig. 1 depicts the XRD patterns of precursors S2-MMT, S3-MMT, and S4-MMT. The presence of MMT in the sample is indicated by the diffraction peaks at 20.23°, 35.29°, 39.6° and 45.9° in Fig. 1 (a), which are consistent with the usual MMT peaks (JCPDS no.

03–0015) indicating MMT presence in the sample [18]. The strong diffraction peaks of S2-MMT, S3-MMT, and S4-MMT indexed to a series of 003, 006, 012, and 015, which corresponds to Mg/Al hydrotalcite-like materials (JCPDS 35–0965) [19]. The presence of metal cations Ni^{+2} and Al^{+3} (JCPDS 15–0087) in the host layer is indicated by peaks with series of 018, 110, and 113 (near $2\theta = 60°$) [20]. For S2-MMT, S3-MMT, and S4-MMT samples, the d-spacing of the plane (003) is approximately 0.759 nm, 0.764 nm, and 0.778 nm, respectively. This XRD pattern result demonstrates that interlayer spacing reduces as Al^{3+} feeding content increases. Table 1 displays the crystal lattice parameters. Fig. 1 (b) shows the XRD pattern for pure S2-LDH, S3-LDH, and S4-LDH.

3.2. Morphological study

The L.D.H. microspheres, which resemble flowers and are stacked together in Fig. 2(a–d), are made up of multiple nanoplatelets crossed over one another. The hierarchical abundant porous structure for S2-MMT is visible in Fig. 2(b), which aids in improving adsorption. The S3-MMT and S4-MMT exhibit the flower-like structure typical of layered double hydroxide [22], with spherical agglomerates and numerous projecting thin 2D nanoflakes Fig. 2(c and d), significantly increasing the active sites for adsorption of dyes. A further indication that pure S2-LDH contains nanometer-sized particles are wrinkles that are several micrometers long Fig. 2(a).

3.3. Pore properties

Fig. 3 shows the low-temperature nitrogen sorption isotherms and pore size distribution (PSD) of the S2-LDH, S2-MMT, S3-MMT, and S4-MMT. With a relative pressure range of 0.7–0.98, the nitrogen adsorption-desorption isotherm for S2-LDH, S2-MMT, and S3-MMT displays type IV hysteresis loop, indicating capillary condensation characteristics [21]. It can also be inferred from Fig. 3(a) that S2-LDH, S2-MMT, and S3-MMT all contain pores that are basically slit-shaped based on the isotherm's type and the hysteresis loop's shape. While S4-MMT exhibits a type III isotherm and has an H4 hysteresis loop that suggests narrow or thin slit pores, The texture characteristics of these samples are summarised in Table 2. S2-LDH, S2-MMT, S3-MMT, and S4-MMT have BET surface areas of 29.03 m^2/g, 40.68 m^2/g, 82.13 m^2/g and 145.6 m^2/g,respectively. According to these findings, L.D.H. grows onto MMT with increasing surface area. According to Groen's study [23], Fig. 3(b) shows the average pore diameters of S2-LDH, S2-MMT, S3-MMT, and S4-MMT are 18 nm, 19 nm, 20 nm, and 29.26 nm, respectively. This indicates the presence of mesopores.

In accordance with the studies (Table 2), S4-MMT possesses the largest BET surface area (145.6 m^2/g) and a nano-flower structure, which can be associated with the composite material generating more layers as the metallic ratio increases. The large porosity and surface area may give additional adsorption active sites.

3.4. FTIR spectra

Fig. 4 shows the FTIR spectra of prepared samples. The high absorption peak at 3526 cm^{-1} is due to the stretching modes of water molecules present in the interlayer and OH groups, whereas the weak signal at 1641 cm^{-1} is due to the bending mode of water molecules [24,25]. According to Z. Sun et al. [26] and dos Santos et al. [27], the peaks at 1360 cm^{-1} show the coexistence of carbonates and nitrates species in L.D.H. galleries, respectively. According to Pourfaraj et al. [28], the other low-frequency bands, 642 cm^{-1}, can be accredited to the stretching lattice vibrational modes of $M - O$, $M - OH$, and O-M-O (where $M = Mg^{2+}$, Ni^{2+}, or Al^{3+}). This explanation is consistent with the XRD characterization.

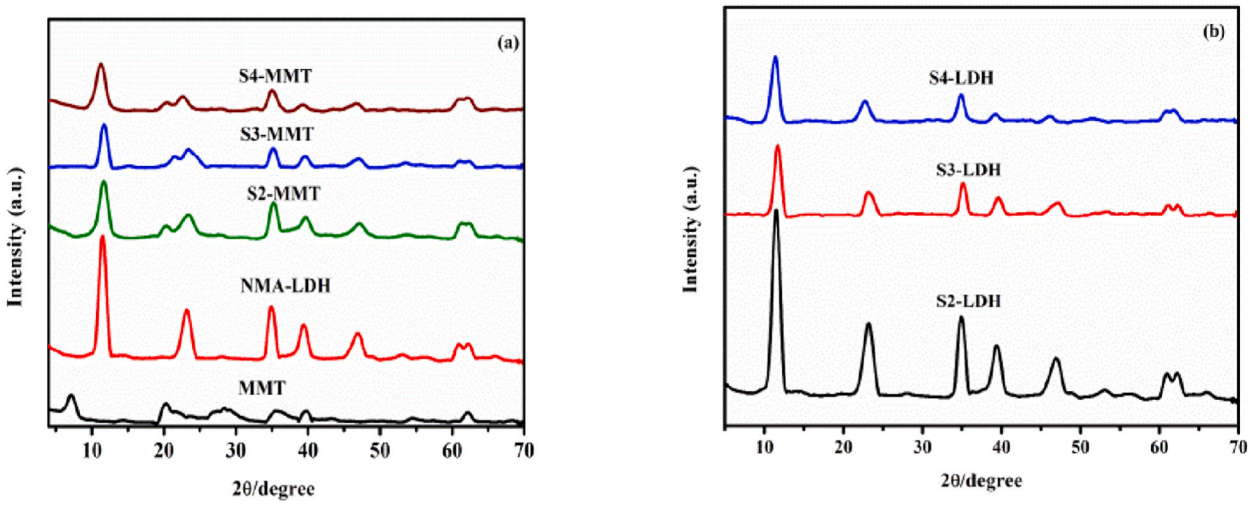

Fig. 1. XRDs of NMA-LDHs modified by MMT and pure MMT (a) XRDs of NMA-LDHs precursor (b) containing different ratios of metals.

Table 1
Characterization data of prepared samples.

Samples	$a = 2d_{110}$ nm	$c = 2d_{003}$ nm	Basal spacing d_{003} nm	Basal spacing d_{110} nm
S2-MMT	0.302	2.277	0.759	0.1510
S3-MMT	0.302	2.292	0.764	0.1510
S4-MMT	0.303	2.334	0.778	0.1519
S2- LDH	0.303	2.286	0.762	0.1518
S3-LDH	0.303	2.295	0.765	0.1518
S4-LDH	0.303	2.35	0.784	0.152

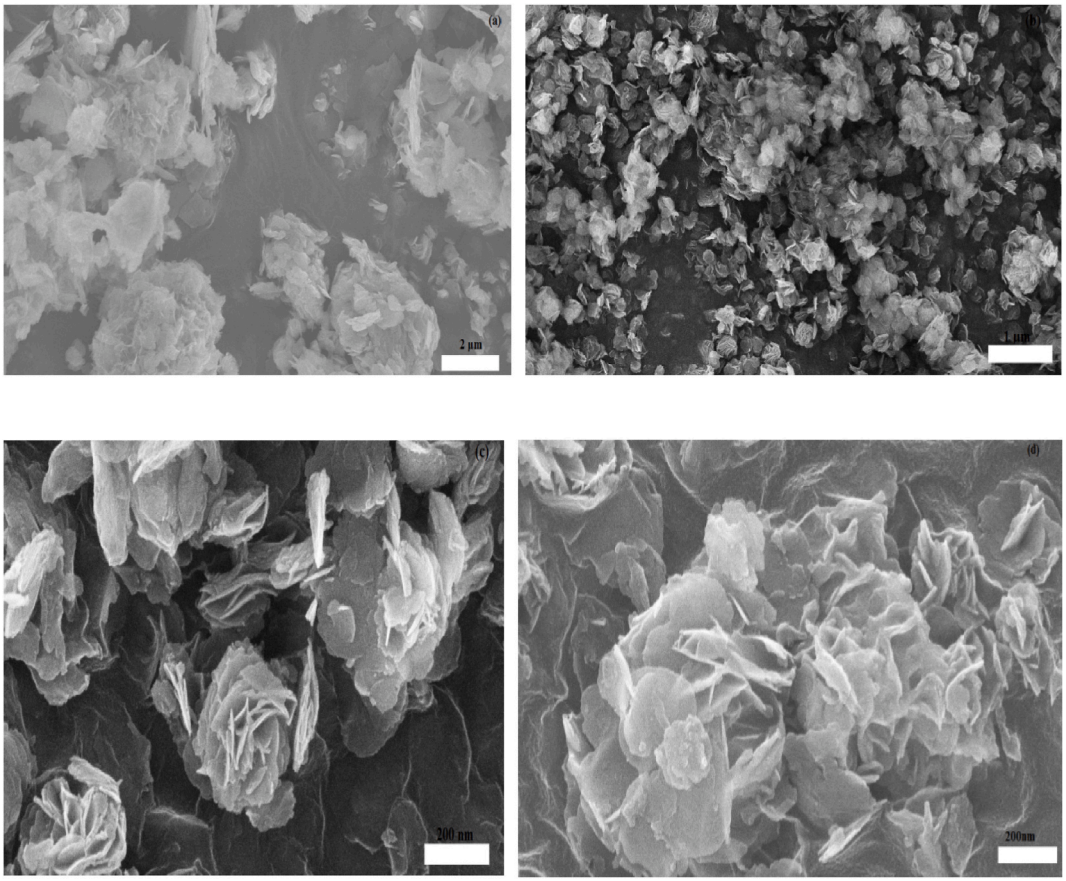

Fig. 2. SEM analysis of S2-LDH (a), S2-MMT (b), S3-MMT (c), S4-MMT (d).

3.5. Adsorption of C.R. And M.B

3.5.1. Effect of Adsorbent dosage

Fig. 5 displays the effect of the dosage of adsorbent on the percentage removal efficiancy (%) for synthesized samples. According to the findings, the percent removal efficiency (%) ranged from 75 to 87 % for S2-LDH, 84–88 % for S2-MMT, 86–93 % for S3-MMT, and 95–97% for S4-MMT for C.R. dye at pH = 2 (Fig. 5(a)) and 82–85 % for S2-LDH, 83–89 % for S2-MMT, 83–91 % for S3-MMT, and 84–92 % for S4-MMT for M.B. dye at pH = 9 (Fig. 5(b)), increased as the dosage of the adsorbent increased. However, the maximum removal capacity (mg/g) decreased. Aggregation limits adsorption sites from being available, which lowers the entire surface area available for additional dye adsorption. The optimal experimental dosage was determined to be 0.01g of adsorbent [29].

3.5.2. pH effect

Fig. 6 illustrates the elimination percent of C.R. and M.B. as a function of pH. It is observed that the highest adsorption of C.R. occurs at pH 2. This is so because the L.D.H.s' positively charged surface at low pH makes them more electrostatically attractive to the anionic dye molecules. In addition, the montmorillonite component can also become protonated at low pH, further enhancing the adsorption of anionic dyes. (Fig. 6(a)). The percent removal was around 97 %.

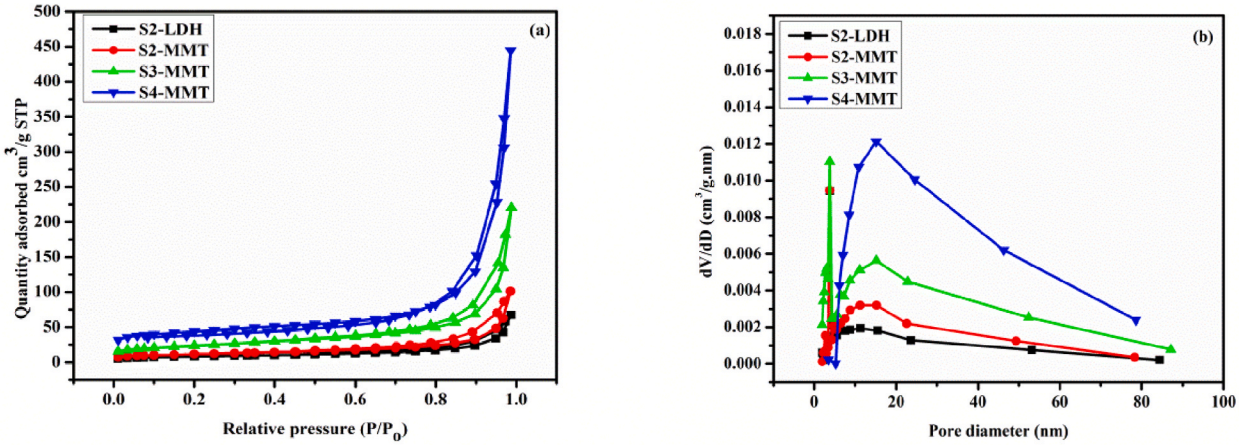

Fig. 3. Isotherms of nitrogen adsorption-desorption (a) and Curves of pore size distribution (b) of each sample.

Table 2
Summarizes the results of pore structure parameters.

Samples	d_{pore} (nm)	V_{pore} (cm^3/g)	S_{BET} (m^2/g)
S2-LDH	18.16	0.0019	29.03
S2-MMT	19.71	0.0034	40.68
S3-MMT	20.26	0.0068	82.13
S4-MMT	29.26	0.0290	145.6

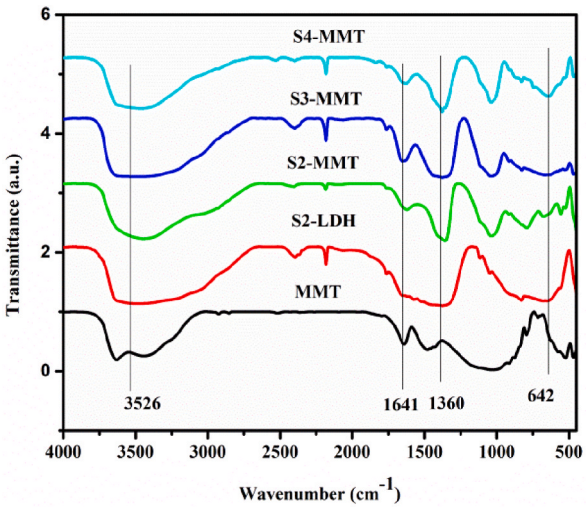

Fig. 4. The FTIR study of as-synthesized samples.

The quantity of M.B. adsorbed (Fig. 6(b)) varied only slightly with pH. At high pH, L.D.H.s can undergo deprotonation of their hydroxyl groups, resulting in a negative surface charge. This negative charge can attract and adsorb cationic dyes due to their positive charge. Also, the quantities adsorbed M.B. was lower than the C.R. values. The percentage removal was around 92 %. Electrostatic interaction between the positively charged cationic dye and the negatively charged surface of the LDH-modified with MMT is involved in the adsorption mechanism. Moreover, the material's increased surface area gives dye molecules more places to interact, boosting adsorption capacity.

3.6. Kinetic studies

Kinetic analysis is important in determining the effect of contact time and the underlying mechanism of adsorption processes [30]. Figs. 7 and 8 show the effect of time on C.R. and M.B. adsorption by the prepared samples S2-LDH, S2-MMT, S3-MMT, and S4-MMT.

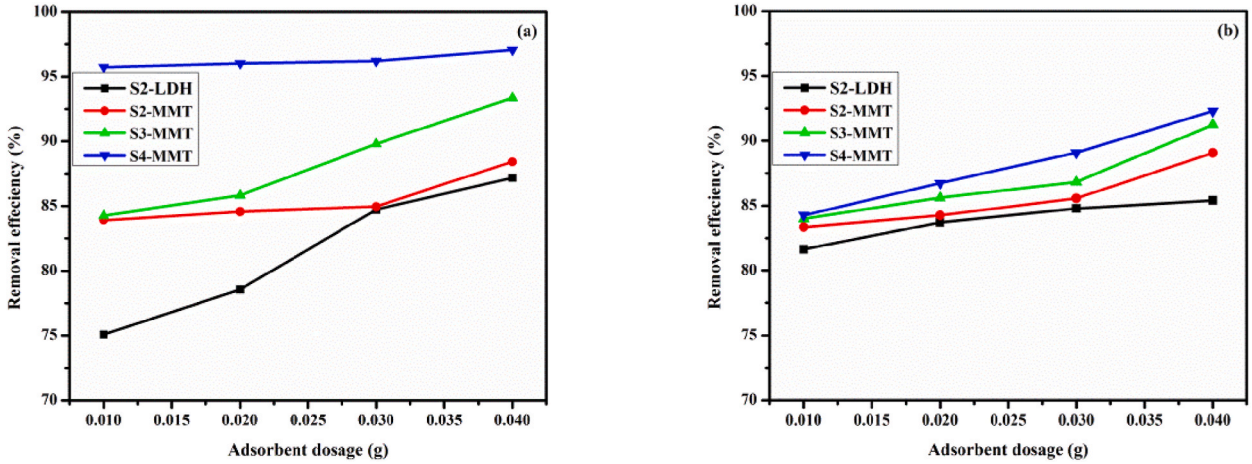

Fig. 5. Effect of Adsorbent dosage when C.R. (a) and M.B. (b) = 25 mg/L, m = 0.01–0.04 g, V = 0.1 L, and at T = 25 ± 1 °C.

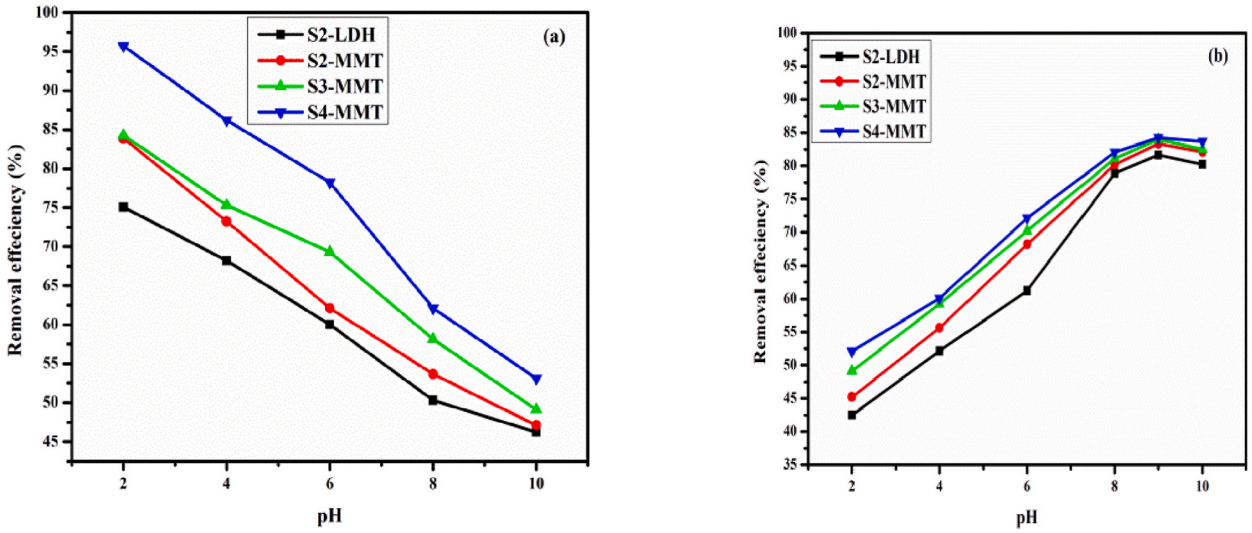

Fig. 6. Effect of pH when C.R. (a) and M.B. (b) = 25 mg/L, V = 0.1 L, m = 0.01 g and at T = 25 ± 1 °C.

Fig. 7 ((a)–(b)) and 8 ((a)-(b)) demonstrate the pseudo-first-order and pseudo-second-order kinetic models that are consistent with the samples for the adsorption of C.R. and M.B. dye under specific conditions. As shown in Table 3, kinetic adsorption better matches the pseudo-second-order model than the experimental values of the calculated q_e, which are nearly equal. These findings show that the pseudo second-order sorption mechanism is dominant and that the sorption process's overall rate constant appears to be governed by a chemisorption process. Figs. 7(c) and 8(c) display the maximum amount adsorbed for all prepared samples as a function of contact time, while the percent removal efficiency is shown in Figs. 7(d) and 8(d). Adsorption occurs rapidly and constantly throughout the first 60 min of the experiment, and all samples reached adsorption equilibrium within approximately the same time (90 min) [31].

3.7. Adsorption isotherm

Figs. 9 and 10 display the adsorption isotherms of C.R. and M.B. with concentrations varying from 5 to 25 mg/L for four prepared samples after 90 min of contact time. Figs. 9 (a) and 10 (a) show the effect of C.R. and M.B. concentration on removal capacity, respectively. The Langmuir adsorption isotherm model is shown in Figs. 9(b)–10(b) of all samples for C.R. and M.B. dye, respectively. The linear Langmuir plot is used to estimate the values of q_{max} and K_L. The Freundlich isotherm constants K_F and n are calculated by the plot between $\ln q_e$ and $\ln C_e$ (Figs. 9(c)–10(c)). Fig. 9(d)–10(d) depict the maximum removal capacity of prepared samples for C.R. and M.B. dye, respectively. Table 4 lists the isotherm parameters examined for the Langmuir and Freundlich models. Regarding R^2, the experimental data more closely match the Langmuir isotherm model than the Freundlich isotherm, demonstrating the homogenous adsorption-controlled process. This demonstrated that the Langmuir isotherm correctly described the characteristics of C.R. and M.B. as well as the sorption mechanism on the composite under investigation.

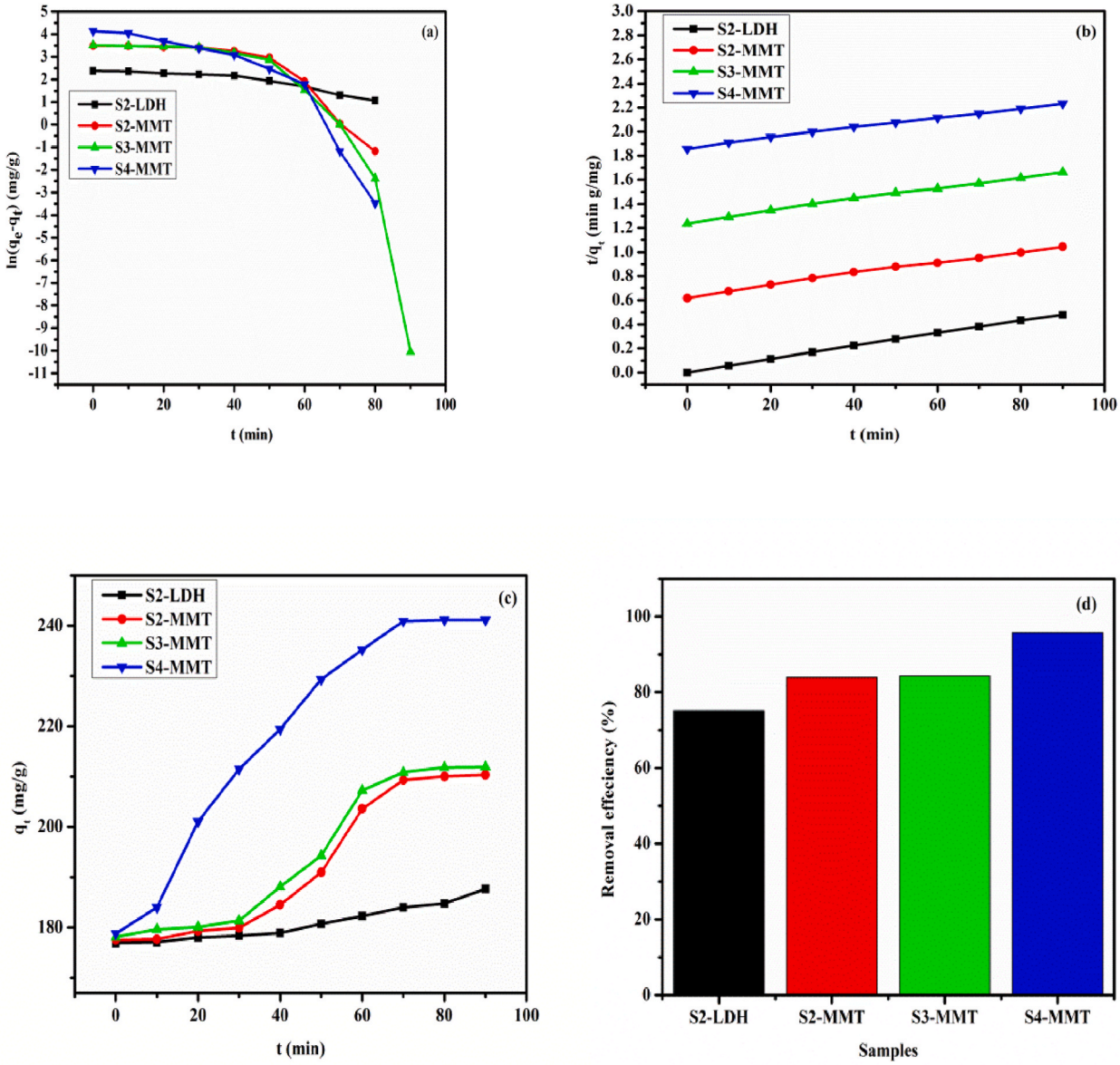

Fig. 7. Pseudo-first-order kinetic model (a) Pseudo-second-order kinetic model (b) Effect of contact time on the maximum amount adsorbed of C.R. dye for as-synthesized samples (c) removal percent (%) of each sample (d) when m = 0.01g, C.R. = 25 mg/L, T = 25 ± 1 °C, V = 0.1 L, and at pH = 2 ± 0.2.

3.8. Regeneration cycles

Regeneration experiments were performed to evaluate the effectiveness, stability, and repeatability of prepared samples. After each cycle, 8 % HNO_3 was used as a desorption agent to remove the M.B. and C.R. dye from the adsorbent. The removal percent (%) reduces from cycle 1 to cycle 4, as shown in Fig. 11. In the very first cycle, the percentage adsorption of C.R. dye (Fig. 11(a)) for adsorbents S2-LDH, S2-MMT, S3-MMT, and S4-MMT was 75 %, 84 %, 86 %, and 95 %, respectively, while the removal of M.B. dye was 82 %, 83 %, 83 %, and 85 %, respectively (Fig. 11(b)). Whereas 50 %, 55 %, 59 %, and 63 % removal percent of C.R. dye and 41 %, 46 %, 51 %, and 58 % removal percent of M.B. dye were observed for adsorbents S2-LDH, S2-MMT, S3-MMT, and S4-MMT, respectively in 4th cycle. The reduction in removal percent (%) can be ascribed to the resultant loss of surface area and the ultimate breakdown of the adsorbent porous structure into a packed structure [32]. The synthesized samples' ability to be reused has been established with complete C.R. and M.B. dye adsorption, which is favorable in its practical wastewater treatment applications [33].

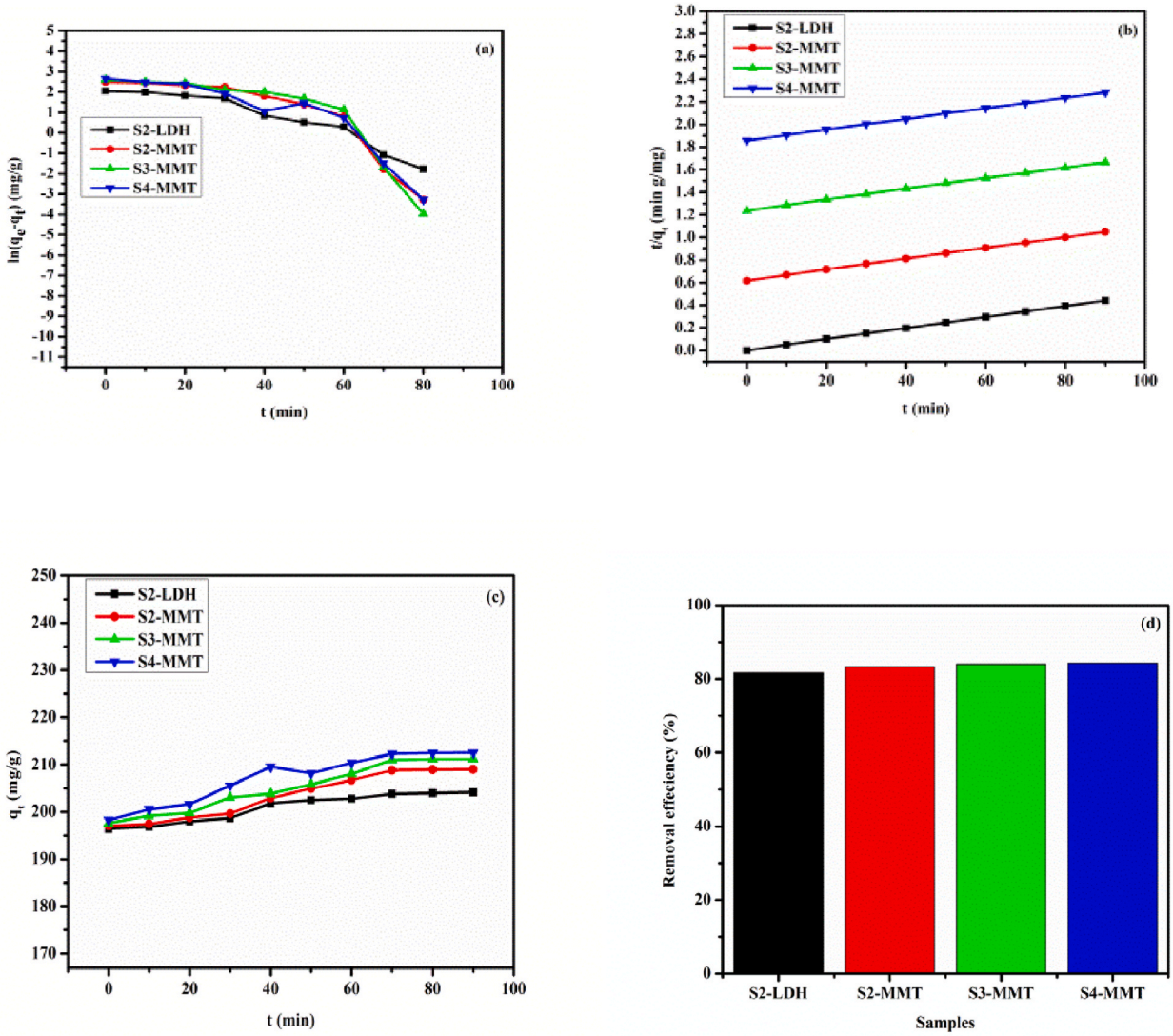

Fig. 8. Pseudo-first-order kinetic model (a) Pseudo-second-order kinetic model (b) Effect of contact time on the maximum amount adsorbed of M.B. dye for as-synthesized samples (c) removal percent (%) of each sample (d) when m = 0.01g, M.B. = 25 mg/L, T = 25 ± 1 °C, V = 0.1 L, and at pH = 9 ± 0.2.

Table 3
Pseudo-first-order and Pseudo-second-order kinetic model parameters of the as-synthesized samples.

Adsorbates	Samples	$q_{e,exp}$ (mg/g)	Pseudo first-order model			Pseudo second-order model		
			$q_{e,cal}$ (mg/g)	k_1 (× 10^{-2} min^{-1})	R2	qe, cal (mg/g)	k_2 (× 10^{-3} g/mg min)	R^2
	S2-LDH	211.4	15.6	5.2	0.773	185.1	5.61	0.9994
	S2-MMT	220.6	83.40	2.25	0.801	207.7	1.44	0.9945
C.R.	S3-MMT	185.5	113.0	1.12	0.628	210	1.45	0.9952
	S4-MMT	228.39	156.0	7.25	0.739	230	1.35	0.9971
	S2-LDH	204.151	10.76	3.87	0.786	202.08	10.2	0.9999
M.B.	S2-MMT	208.38	25.35	5.1	0.660	207.7	5.42	0.9997
	S3-MMT	209.96	29.95	5.6	0.612	209	5.02	0.9996
	S4-MMT	210.63	35.23	5.26	0.689	210	6.188	0.9998

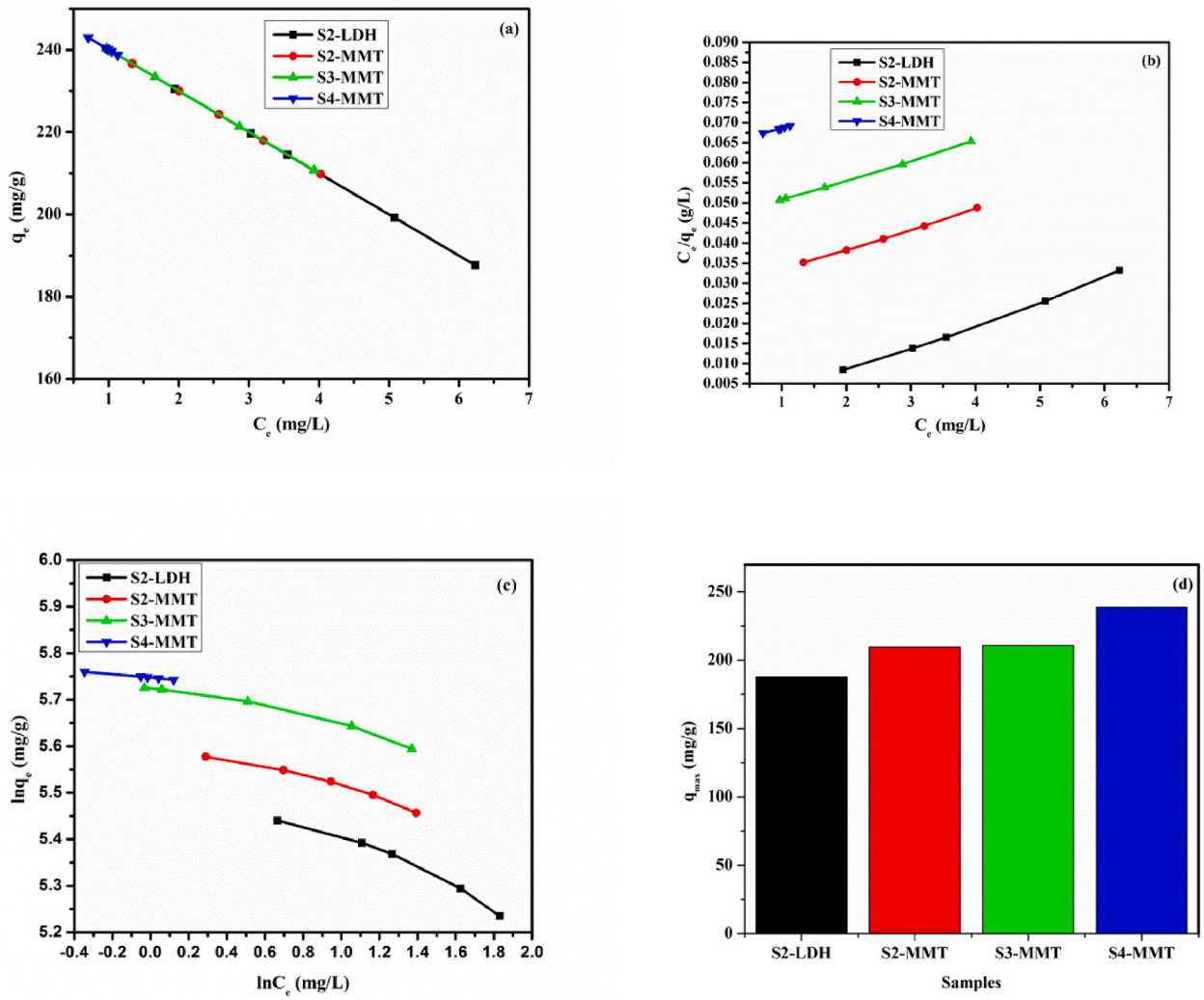

Fig. 9. Equilibrium adsorption isotherms, the effect of C.R. concentration on maximum amount adsorbed (a), Langmuir Model (b), Freundlich Model (c) maximum quantity adsorbed of synthesized samples (d) when the C.R. concentration was 5–25 mg/L, m = 0.01g, V = 0.1 L, T = 25 ± 1 °C and at pH = 2 ± 0.2 (without adjusting the initial pH).

4. Conclusions

We report the synthesis of NMA-LDHs (S2-LDH, S3-LDH, and S4-LDH) and MMT-modified L.D.H.s (S2-MMT, S3-MMT, and S4-MMT) via a one-step hydrothermal method. The distinctive XRD studies made available in this work are supported by helpful kinetic and mechanistic explanations. The chemical ratio of metals in the modified L.D.H.s is directly related to the adsorption effectiveness towards C.R. and M.B. In contrast to the sample without MMT (S2-LDH), the sample with MMT (S4-MMT) only demonstrated substantial adsorption capabilities for C.R. and M.B. (344 mg/g and 200 mg/g, respectively). It is an established fact that hierarchical nano-flower structures, with mesoporous morphology and high surface area, have numerous adsorptive sites for the adsorption process, which is in accordance with our results. The best dosage and contact duration for prepared samples were 0.01 g and 90 min, respectively. The pH studies revealed that the maximum C.R. adsorption occurs at pH 2 while the maximum M.B. adsorption occurs at pH 9. The adsorption kinetics of all samples adsorbing C.R. and M.B. dyes were established to follow the pseudo-second-order model. The findings from the adsorption isotherm model fit the Langmuir model well. The prepared samples could be arranged according to maximum Langmuir adsorption capacity in the order: S4-MMT > S3-MMT > S2-MMT > S2-LDH. For C.R. and M.B., the highest adsorption capacity q_{max} of S4-MMT was 344 mg/g and 200 mg/g, respectively. Furthermore, the adsorption-desorption cycles show that the produced samples are reusable and stable. All of the results suggested that NMA-LDHs modified with MMT could be used as a reliable, cost-effective, and alternative adsorbent for eliminating dyes from wastewater.

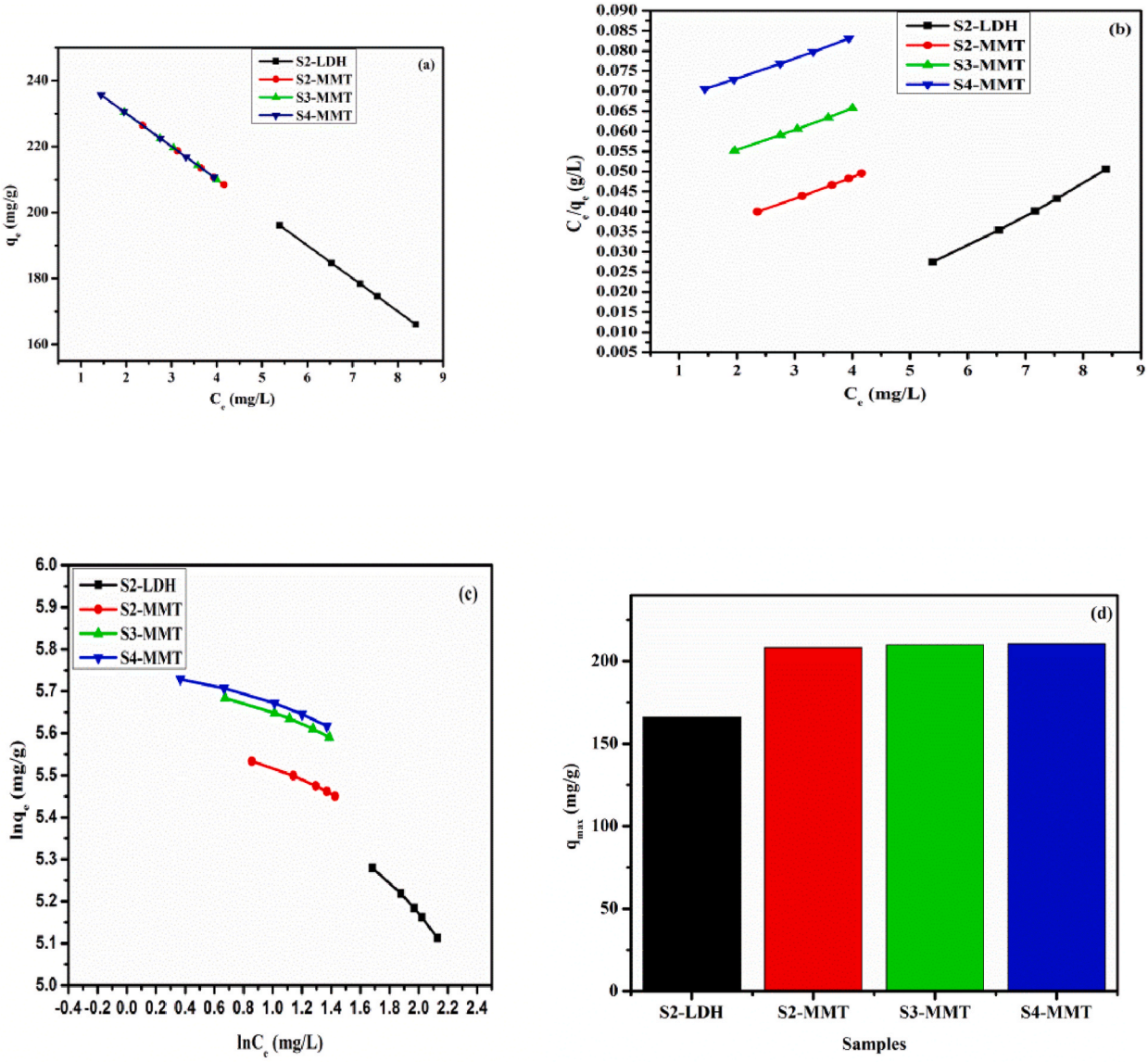

Fig. 10. Equilibrium adsorption isotherms, the effect of M.B. concentration on maximum amount adsorbed (a), Langmuir Model (b), Freundlich Model (c) maximum quantity adsorbed of synthesized samples (d) when the M.B. concentration was 5–25 mg/L, V = 0.1 L, T = 25 ± 1 °C, m = 0.01g and at pH = 9 ± 0.2 (without adjusting the initial pH).

Table 4
The Langmuir and Freundliich isotherm Model constants of the as-synthesized samples.

Adsorbate	Samples	Langmuir isotherm model			Freundlich isotherm model		
		q_{max} (mg/g)	K_L (L/mg)	R^2	KF(mg/g) (L/mg)1/n	n	R^2
C.R.	S2-LDH	172.41	1.62	0.996	263.59	5.68	0.991
	S2-MMT	263.15	1.90	0.990	246.16	9.29	0.988
	S3-MMT	303.03	3.67	0.998	241.29	11.01	0.991
	S4-MMT	344	5.61	1	239.91	27.24	0.985
M.B.	S2-LDH	131.57	1.81	0.996	368.15	2.69	0.99
	S2-MMT	188.67	2.52	0.999	256.95	6.91	0.991
	S3-MMT	192.30	3.06	0.999	252.2	7.78	0.983
	S4-MMT	200	3.84	0.999	246.8	9.17	0.977

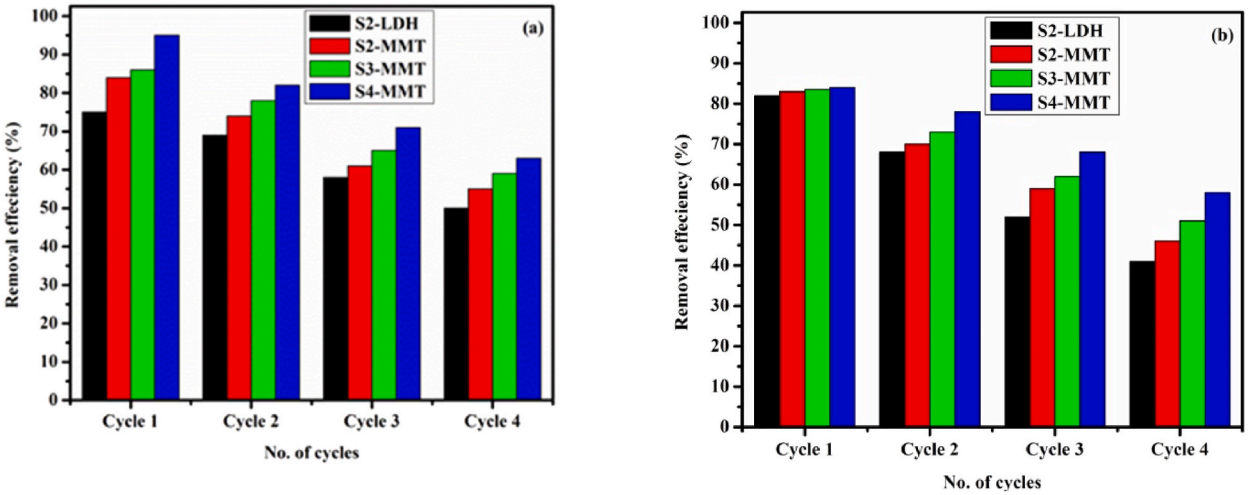

Fig. 11. The Reusability of adsorbents for the adsorption of C.R. (a) and M.B. (b) in four adsorption-desorption cycles when C.R. and M.B. dyes = 25 mg/L, V = 0.1 L, m = 1 g, T = 25 ± 1 °C and at pH = 2 ± 0.2 for C.R. and at pH = 9 ± 0.2 for M.B.

Data availability statement

The manuscript covers all of the data.

CRediT authorship contribution statement

Tayyaba Waheed: Data curation, Investigation, Project administration, Writing – original draft. **Pu Min:** Conceptualization, Data curation, Resources, Software, Visualization. **Salah ud Din:** Data curation, Project administration, Software, Supervision, Validation. **Pervaiz Ahmad:** Conceptualization, Investigation, Resources, Validation, Visualization. **Mayeen Uddin Khandaker:** Data curation, Funding acquisition, Software, Validation, Visualization. **Sirajul Haq:** Conceptualization, Data curation, Software, Supervision, Writing – review & editing. **K.S. Al-Mugren:** Formal analysis, Funding acquisition, Project administration, Resources, Validation, Visualization. **Fazal Ur Rehman:** Data curation, Formal analysis, Project administration, Resources, Supervision. **Bilal Akram:** Conceptualization, Software, Validation, Visualization, Writing – review & editing. **Sehrish Nazir:** Conceptualization, Data curation, Methodology.

Declaration of competing interest

The authors declare the following financial interests/personal relationships which may be considered as potential competing interests:K. S. Al-mugren reports financial support was provided by Princess Nourah bint Abdulrahman University. K. S. Al-mugren reports a relationship with Princess Nourah bint Abdulrahman University that includes: employment and funding grants.

Acknowledgments

The authors thank the Princess Nourah bint Abdulrahman University Researchers Supporting Project number (PNURSP2023R10), Princess Nourah bint Abdulrahman University, Riyadh, Saudi Arabia, for their assistance.

References

[1] A. Elhalil, W. Boumya, A. Machrouhi, R. Elmoubarki, S. Mansouri, M. Sadiq, M. Abdennouri, N. Barka, Applied Surface Science Advances Synthesis , characterization and efficient photocatalytic properties of spinel materials for dye degradation, Appl. Surf. Sci. Adv. 13 (November 2022) (2023), 100381.
[2] M. El Mouftari, F.Z. Mahjoubi, F. Kzaiber, W. Terouzi, G.A.M. Ali, S. Souhassou, A. Oussama, Study of oleaster oil's falsification by ATR-FTIR and chemometrics tools, Egypt. J. Chem. 64 (6) (2021) 2747–2755.
[3] S. Dardouri, S. Jalila, A comparative study of adsorption and regeneration with different agricultural wastes as adsorbents for the removal of methylene blue from aqueous solution, Chin. J. Chem. Eng. 25 (9) (2017) 1282–1287.
[4] X. Dai, H. Zeng, C. Jin, J. Rao, X. Liu, RSC Advances toward Growing ZnO for Advanced Photocatalytic Degradation of Methylene Blue †, 2021, pp. 38505–38514.
[5] T. Ting, K. Lin, X. Long, F. Li, J. Mu, Y. Xin, Journal of Physics and Chemistry of Solids Facile decolorization of methylene blue by morphology-dependence δ -MnO 2 nanosheets -modi fi ed diatomite 87 (2015) 196–202.
[6] A.K. Prajapati, M.K. Mondal, Comprehensive kinetic and mass transfer modeling for methylene blue dye adsorption onto CuO nanoparticles loaded on nanoporous activated carbon prepared from waste coconut shell, J. Mol. Liq. 307 (2020), 112949.
[7] N. Ali, A. Said, F. Ali, F. Raziq, Z. Ali, M. Bilal, L. Reinert, T. Begum, H.M.N. Iqbal, Photocatalytic degradation of Congo red dye from aqueous environment using cobalt ferrite nanostructures: development, characterization, and photocatalytic performance, Water. Air. Soil Pollut. 231 (2) (2020).
[8] M. Harja, G. Buema, D. Bucur, Recent advances in removal of Congo Red dye by adsorption using an industrial waste, Sci. Rep. 12 (1) (2022) 1–18.

[9] A.E.-A.A. Said, A.A.M. Aly, M.M.A. El-Wahab, S.A. Soliman, A.A.A. El-Hafez, V. Helmey, M.N. Goda, Application of modified bagasse as a biosorbent for reactive dyes removal from industrial wastewater, J. Water Resour. Prot. 5 (7) (2013) 10–17.
[10] M. Farnane, H. Tounsadi, A. Machrouhi, A. Elhalil, F.Z. Mahjoubi, M. Sadiq, M. Abdennouri, S. Qourzal, N. Barka, Dye removal from aqueous solution by raw maize corncob and h3po4 activated maize corncob, J. Water Reuse Desalin. 8 (2) (2018) 214–224.
[11] E.K. Aziz, R. Abdelmajid, L.M. Rachid, E.H. Mohammadine, Adsorptive removal of anionic dye from aqueous solutions using powdered and calcined vegetables wastes as low-cost adsorbent, Arab J. Basic Appl. Sci. 25 (3) (2018) 93–102.
[12] A. Machrouhi, N. Taoufik, H. Tounsadi, Z. Rais, Patent Blue V Dye Adsorption by Fresh and Calcined Zn/Al LDH : Effect of Process Parameters and Experimental Design Optimization, 2022.
[13] G. Starukh, O. Rozovik, O. Oranska, Organo/Zn-Al LDH nanocomposites for cationic dye removal from aqueous media, Nanoscale Res. Lett. 11 (1) (2016).
[14] F. Zahra, A. Khalidi, A. Elhalil, Characteristics and mechanisms of methyl orange sorption onto Zn/Al layered double hydroxide intercalated by dodecyl sulfate anion, Sci. African 6 (2019), e00216.
[15] D. Bin Jiang, C. Jing, Y. Yuan, L. Feng, X. Liu, F. Dong, B. Dong, Y.X. Zhang, 2D-2D growth of NiFe LDH nanoflakes on montmorillonite for cationic and anionic dye adsorption performance, J. Colloid Interface Sci. 540 (2019) 398–409.
[16] T. Taher, A. Munandar, N. Mawaddah, M. Syamsuddin Wisnubroto, P.M.S.B.N. Siregar, N.R. Palapa, A. Lesbani, Y.G. Wibowo, Synthesis and characterization of montmorillonite – mixed metal oxide composite and its adsorption performance for anionic and cationic dyes removal, Inorg. Chem. Commun. 147 (October 2022) (2023), 110231.
[17] F.A. Alnasrawi, A.A. Mohammed, Enhancement of Cd2+ removal on CuMgAl-layered double hydroxide/montmorillonite nanocomposite: kinetic, isotherm, and thermodynamic studies, Arab. J. Chem. 16 (2) (2023), 104471.
[18] F.A. Alnasrawi, A.A. Mohammed, T.J. Al-Musawi, Synthesis, characterization and adsorptive performance of CuMgAl-layered double hydroxides/montmorillonite nanocomposite for the removal of Zn(II) ions, Environ. Nanotechnol. Monit. Manag. 19 (May 2023), 100771.
[19] T. Waheed, S. Din, L. Ming, P. Ahmad, P. Min, S. Haq, Porous Hierarchical Ni/Mg/Al Layered Double Hydroxide for Adsorption of Methyl Orange from Aqueous Solution, 2023.
[20] M. Liu, J. Xu, B. Cheng, W. Ho, J. Yu, Synthesis and Adsorption Performance of Mg(OH)2 Hexagonal Nanosheet-Graphene Oxide Composites, 332, Elsevier B.V., 2015.
[21] K. El Hassani, B.H. Beakou, D. Kalnina, E. Oukani, A. Anouar, Effect of morphological properties of layered double hydroxides on adsorption of azo dye Methyl Orange: a comparative study, Appl. Clay Sci. 140 (2017) 124–131.
[22] A. Aurich, J. Hofmann, R. Oltrogge, M. Wecks, R. Gläser, L. Blömer, S. Mauersberger, R.A. Müller, D. Sicker, A. Giannis, Improved isolation of microbiologically produced (2R,3S)-Isocitric acid by adsorption on activated carbon and recovery with methanol, Org. Process Res. Dev. 21 (6) (2017) 866–870.
[23] S. Abelló, J. Pérez-Ramírez, Steam activation of Mg-Al hydrotalcite. Influence on the properties of the derived mixed oxides, Microporous Mesoporous Mater. 96 (1–3) (2006) 102–108.
[24] Z. Sun, C. Lin, J. Zheng, L. Wang, J. Zhang, F. Xu, J. Hou, Fabrication and characterization of hierarchical Mg/Ni/Al layered double hydroxide framework on aluminum foam, Mater. Lett. 113 (3) (2013) 83–86.
[25] C. Lei, X. Zhu, B. Zhu, C. Jiang, Y. Le, J. Yu, Superb adsorption capacity of hierarchical calcined Ni/Mg/Al layered double hydroxides for Congo red and Cr(VI) ions, J. Hazard Mater. 321 (2017) 801–811.
[26] Y. Sun, S. Yang, G. Zhao, Q. Wang, X. Wang, Adsorption of polycyclic aromatic hydrocarbons on graphene oxides and reduced graphene oxides, Chem. Asian J. 8 (11) (2013) 2755–2761.
[27] R.M.M. dos Santos, R.G.L. Gonçalves, V.R.L. Constantino, L.M. da Costa, L.H.M. da Silva, J. Tronto, F.G. Pinto, Removal of Acid Green 68:1 from aqueous solutions by calcined and uncalcined layered double hydroxides, Appl. Clay Sci. 80–81 (2013) 189–195.
[28] R. Pourfaraj, S.J. Fatemi, S.Y. Kazemi, P. Biparva, Synthesis of hexagonal mesoporous MgAl LDH nanoplatelets adsorbent for the effective adsorption of Brilliant Yellow, J. Colloid Interface Sci. 508 (2017) 65–74.
[29] Á. Crini, P. Badot, Application of chitosan , a natural aminopolysaccharide , for dye removal from aqueous solutions by adsorption processes using batch studies : A review of recent literature 33 (2008) 399–447.
[30] R. Chen, J. Yu, W. Xiao, Hierarchically porous MnO2 microspheres with enhanced adsorption performance, J. Mater. Chem. A 1 (38) (2013) 11682–11690.
[31] P. Kowalik, M. Konkol, M. Kondracka, W. Próchniak, R. Bicki, P. Wiercioch, Memory effect of the CuZnAl-LDH derived catalyst precursor - in situ XRD studies, Appl. Catal. Gen. 464 (465) (2013) 339–347.
[32] S.O. Ganiyu, T.X. Huong Le, M. Bechelany, G. Esposito, E.D. Van Hullebusch, M.A. Oturan, M. Cretin, A hierarchical CoFe-layered double hydroxide modified carbon-felt cathode for heterogeneous electro-Fenton process, J. Mater. Chem. A 5 (7) (2017) 3655–3666.
[33] R. Huang, Adsorption of methyl orange onto protonated cross-linked chitosan, Arab. J. Chem. (2013).